Aerosol indirect effects in POLDER satellite data and the Laboratoire de Météorologie Dynamique–Zoom (LMDZ) general circulation model

J. Quaas
Laboratoire de Météorologie Dynamique, IPSL, CNRS-UPMC, Paris, France

O. Boucher
Laboratoire d'Optique Atmosphérique, CNRS-USTL, Villeneuve d'Ascq, France

F.-M. Bréon
Laboratoire des Sciences du Climat et de l'Environnement, IPSL, CEA-CNRS, Gif sur Yvette, France

Received 3 November 2003; revised 31 January 2004; accepted 3 March 2004; published 22 April 2004.

[1] The POLDER-1 instrument was able to measure aerosol and cloud properties for eight months in 1996–1997. We use these observational data for aerosol concentration (the aerosol index), cloud optical thickness, and cloud droplet effective radius to establish statistical relationships among these parameters in order to analyze the first and second aerosol indirect effects. We also evaluate the representation of these effects as parameterized in the Laboratoire de Météorologie Dynamique–Zoom (LMDZ) general circulation model. We find a decrease in cloud top droplet radius with increasing aerosol index in both the model and the observations. Our results are only slightly changed if the analysis is done at fixed cloud liquid water path (LWP) instead of considering all LWP conditions. We also find a positive correlation between aerosol index and cloud liquid water path, which is particularly pronounced over the Northern Hemisphere midlatitudes. This may be interpreted as observational evidence for the second aerosol indirect effect on a large scale. The model-simulated relationship agrees well with that derived from POLDER data. Model simulations show a rather small change in the two relationships if preindustrial rather than present-day aerosol distributions are used. However, when entirely switching off the second aerosol indirect effect in our model, we find a much steeper slope than we do when including it. *INDEX TERMS:* 0320 Atmospheric Composition and Structure: Cloud physics and chemistry; 0305 Atmospheric Composition and Structure: Aerosols and particles (0345, 4801); 1610 Global Change: Atmosphere (0315, 0325); 1640 Global Change: Remote sensing; 1803 Hydrology: Anthropogenic effects; *KEYWORDS:* indirect effects, aerosol, clouds

Citation: Quaas, J., O. Boucher, and F.-M. Bréon (2004), Aerosol indirect effects in POLDER satellite data and the Laboratoire de Météorologie Dynamique–Zoom (LMDZ) general circulation model, *J. Geophys. Res.*, *109*, D08205, doi:10.1029/2003JD004317.

1. Introduction

[2] The possible adverse effects of global change are challenging climate scientists who seek to understand and possibly predict its functioning. Besides the greenhouse effect caused by greenhouse gases, aerosols are considered to constitute the most important anthropogenic perturbation of the climate system. The change in the Earth's energy balance due to aerosols is much more uncertain than that due to greenhouse gases. However, it may be of comparable magnitude even on the global scale, but of opposite sign [*Boucher and Haywood*, 2001].

[3] Tropospheric aerosols have a relatively short lifetime of about a week. For this reason, aerosol impacts on climate vary strongly in space and time. In addition to the direct radiative effect of aerosols (i.e., the extinction of sunlight by scattering and absorption) aerosols interact with clouds and subsequently with radiation. Two modes of functioning of these so-called aerosol indirect effects (AIE) are distinguished. By their ability to act as cloud condensation nuclei (CCN), an increase in aerosol concentration causes an increase in cloud droplet number concentration (CDNC) for the same amount of cloud water. This effect, which increases the cloud albedo, is called the first AIE [*Twomey*, 1974]. The cloud microphysical processes, by which precipitation is formed, depend on the size of the cloud particles. Smaller droplets are less likely to coalesce, so the cloudiness is less efficiently decreased. The resulting increase in cloud lifetime and cloud cover is likely to cause a net cooling of the climate system. This is called the second AIE [*Albrecht*, 1989]. To understand the aerosol-cloud

0148-0227/04/2003JD004317$09.00

interactions on a global scale, the most promising approach is the combination of general circulation models (GCMs) and satellite measurements. GCMs include the treatment of a multitude of dynamical and physical processes and are able to simulate interactions between many climate parameters. Comparing the results of different simulations is a powerful method to understand climate processes. In contrast to observations, the impacts of single processes can be isolated. A disadvantage of GCMs is their coarse resolution. Observations with spaceborne instruments are the only measurements which cover the whole globe on long timescales. Satellite observations can therefore be used to evaluate GCM simulations. Current satellite instruments generally measure top-of-the-atmosphere radiances in the shortwave and longwave spectrum, thus providing a two-dimensional (latitude-longitude) view of cloud properties but with limited information on the vertical distribution.

[4] Using AVHRR satellite observations, *Wetzel and Stowe* [1999] showed an inverse relationship between zonal and seasonal averages of aerosol optical depth and droplet size of stratus clouds over oceans. They also found an increase in seasonal and zonal mean cloud optical thicknesses with increasing aerosol optical thickness over oceans. *Schwartz et al.* [2002] used a combination of a hemispheric model and AVHRR satellite data to study the correlations between modeled aerosol data and satellite-derived cloud properties for a period of one week in April 1987 over the North Atlantic Ocean. They found a negative correlation between simulated sulfate aerosol concentration and observed cloud droplet radius, but no correlation between simulated sulfate and observed cloud optical depth. Again from AVHRR data, *Nakajima et al.* [2001] derived a negative correlation between cloud droplet effective radius and aerosol column number concentration over oceans. *Sekiguchi et al.* [2003] extended this work to study the dependence of the correlation slopes on the spatial and temporal averaging and to evaluate the effects of aerosols on the cloud structure (cloud height and cloud fraction). They found a positive slope between cloud optical depth and aerosol column number concentration.

[5] *Bréon et al.* [2002] used POLDER data to establish a relationship between quasi colocated aerosol properties and cloud droplet effective radii (CDR). They put in evidence the first aerosol indirect effect by identifying a decrease in cloud droplet effective radii with increasing aerosol concentrations. *Lohmann and Lesins* [2002] compared these data with results from simulations with the ECHAM GCM to investigate the relative importance of the first and second AIE in their model. They found a too steep decrease in effective radius with increasing aerosol burden if the second indirect effect was excluded. *Lohmann and Lesins* [2003] extended this study and further found an increase in LWP with increasing aerosol index in their model. They showed that independently of the LWP, the CDR to aerosol index relationship is different in maritime compared to continental conditions. *Rosenfeld and Feingold* [2003] challenged the results of *Bréon et al.* [2002] and the comparison of satellite- and model-based relationships. We will address some of their comments in sections 4 and 5.

[6] In contrast to previous studies exploiting satellite observations (with the exception of *Bréon et al.* [2002] and *Sekiguchi et al.* [2003]), we do not average cloud and aerosol parameters over large regions and long timescales; rather we seek relationships between parameters derived from colocated (within a few degrees' resolution) and simultaneous measurements. A second difference from former studies is that we try to distinguish the aerosol impact on clouds for different cloud liquid water paths. *Han et al.* [1998, 2002] showed different behaviors of the relationship between cloud droplet column concentration and cloud optical thickness, τ, for small ($\tau < 15$) and large ($\tau > 15$) cloud optical thicknesses.

[7] In this study, we exploit satellite data from the Polarization and Directionality of the Earth's Reflectances (POLDER) instrument and the Laboratoire de Météorologie Dynamique–Zoom (LMDZ) GCM. We establish statistical relationships in both satellite observations and results from model simulations to understand both the first and second AIE and to isolate the contribution of anthropogenic aerosols.

2. Observational Data From POLDER

[8] The POLDER-1 spaceborne radiometer on board the Japanese ADEOS satellite was able to measure various aerosol and cloud properties [*Deuzé et al.*, 1999; *Buriez et al.*, 1997] for the period from November 1996 until June 1997. Additionally, *Bréon and Goloub* [1998] showed that in some cases multidirectional polarized radiance measurements can be inverted to estimate the CDR at cloud top. Their method unambiguously derives the size of spherical water droplets. This is an advantage compared to other methods to derive CDR which could be contaminated by aerosol layers above clouds [*Haywood and Osborne*, 2004]. This retrieval was performed by *Bréon and Colzy* [2000], who derived CDR at cloud top for the whole POLDER-1 period in cases of horizontally homogeneous liquid clouds on a scale of at least 150×150 km^2. We will be using the cloud optical thickness, τ_c, derived over land and ocean [*Buriez et al.*, 1997] and the CDR described above.

[9] We use the POLDER aerosol index (AI) derived over land and ocean [*Deuzé et al.*, 1999]. The AI is estimated as the product of the aerosol optical depth, τ_a, and the Ångström coefficient, α, which is a measure of the particle size. It is therefore noted $\alpha\tau$ and may be interpreted as the load of submicronic aerosols. Recent studies have shown a high correlation between the AI and the column-integrated CCN concentration [*Nakajima et al.*, 2001].

[10] We interpolate all observational data to the coarser GCM grid. In contrast to *Bréon et al.* [2002], who use back-trajectories to relate a particular measurement of CDR to a clear-sky (upwind) measurement of aerosols, we correlate here the aerosol and cloud parameters in the same grid box. This should be adequate, as the model grid boxes are much larger than the POLDER pixels.

[11] As there is no direct derivation of LWP from POLDER measurements, we estimate it from the cloud optical thickness, τ_c, and the CDR, r_e, by inverting the equation for τ_c [*Stephens*, 1978]:

$$\tau_c = \frac{3}{2}\frac{\mathrm{LWP}}{r_e\,\rho_w}, \tag{1}$$

where ρ_w is the density of liquid water. Thus we get a measurement of LWP only over grid boxes where a

measurement of the CDR exists, i.e., for homogeneous liquid clouds.

3. Model Description and Derivation of a "Satellite-Like" Model Output

[12] We use the Laboratoire de Météorologie Dynamique–Zoom (LMDZ) GCM [*Li*, 1999]. The GCM is run at a resolution of 96 × 73 points on a regular longitude-latitude horizontal grid with 19 hybrid sigma coordinate levels. In the model, a "dynamics" part, which solves the primitive equations, and a "physics" part, which includes the relevant subgrid-scale physical processes, may be distinguished. The time step of the model is 6 min for the dynamical part of the model and 30 min for the physics. Concerning the physics, radiative transfer is based on the scheme of *Fouquart and Bonnel* [1980] for the solar spectrum and on an updated version of *Morcrette* [1991] in the terrestrial part. Convection is parameterized in the model using the Tiedtke scheme [*Tiedtke*, 1989].

[13] Condensation of water vapor is calculated using a "hat" probability density function for total water content to allow for fractional cloudiness [*Le Treut and Li*, 1991]. We apply the microphysical scheme of *Boucher et al.* [1995], which includes autoconversion and accretion for liquid water clouds and a fall-velocity-dependent snow formation equation for ice clouds. The CDNC (in cm^{-3}) is diagnosed from aerosol mass concentration, m_a (in $\mu g\ m^{-3}$), using the empirical formula of *Boucher and Lohmann* [1995] (formula "D"):

$$N_d = 10^{a_0 + a_1 \log(m_a)}, \tag{2}$$

where the empirical constants are $a_0 = 2.21$ and $a_1 = 0.41$. The LMDZ model includes a comprehensive online sulfur cycle model [*Boucher et al.*, 2002] as well as atmospheric cycles of sea-salt, organic matter, black carbon, and dust aerosols (M. S. Reddy and O. Boucher, A study of the global cycle of carbonaceous aerosols in the LMDZT general circulation model, submitted to *Journal of Geophysical Research*, 2004). In contrast to *Boucher and Lohmann* [1995], who used the mass of sulfate aerosols as a surrogate for all aerosols, we use here instead the maximum of the masses of the three hydrophilic aerosol species considered in the model (sulfate, hydrophilic organic matter, and submicronic sea salt). This modification has an influence on cloud properties in biomass burning regions but a very small one in the Northern Hemisphere, where sulfate concentrations dominate. The volume-mean cloud droplet radius for liquid water clouds is calculated assuming spherical particles:

$$r_d = \sqrt[3]{\frac{q_l\ \rho_{\mathrm{air}}}{(4/3)\ \pi \rho_w N_d}}, \tag{3}$$

where q_l is the cloud liquid water mixing ratio, ρ_{air} is the air density, ρ_w is the density of liquid water, and N_d is the CDNC. The volume-mean cloud droplet radius is related to the cloud droplet effective radius in our model as $r_e = 1.1\ r_d$. While the first AIE causes the CDR to decrease, the second AIE results in an increase in cloud liquid water content, q_l. Both effects cause an increase in cloud optical thickness, which is parameterized as in equation (1).

[14] We simulate the whole period of the POLDER-1 measurements (1 November 1996 to 29 June 1997), starting two months before to allow for a spin-up of the aerosol concentrations. The SST and sea ice are imposed using the SST data set of *Reynolds and Smith* [1995] and the HADISST1.1 sea ice data of the Hadley Centre [*Rayner et al.*, 2003]. We nudge the model horizontal winds and temperature to ECMWF reanalysis data using relaxation times of 0.1 day for the winds and 1 day for the temperature in order to get realistic meteorological conditions. We simulate online in the model the POLDER swath to sample aerosols and clouds properties in the model in the same way the satellite does it. Therefore we do not expect any bias due to differences in sampling the diurnal cycle in the model and satellite data.

[15] Cloud top quantities are estimated as seen by the satellite using the random cloud overlap assumption. By doing so, we account for the contribution of each layer to the two-dimensional distribution seen at each grid point and time step from above. For the effective radius, only liquid water clouds that are not covered by clouds in layers above are considered. To match the POLDER criterion of horizontally homogeneous clouds at 150 × 150 km^2 resolution, we only perform the estimation when at least a quarter of the grid box is covered by a liquid cloud. As a model grid box is 3.75 × 2.5° large, this matches approximately the resolution of the satellite data at least near the equator. (The model results are not very sensitive to the choice of this threshold.) The optical thickness of liquid clouds is calculated using the ISCCP simulator [*Webb et al.*, 2001].

[16] To be consistent with the derivation of LWP from the POLDER data, we also invert the LWP in the model from equation (1) using the above-derived optical thickness and cloud top droplet radius of liquid clouds. This is expected to give an upper bound to the LWP, as τ_c is an integrated value while r_e is the cloud top droplet effective radius. As in general r_e increases with height in a cloud, the cloud top value is expected to be largest. For the model output, the LWP calculated this way is compared to the LWP directly computed from the liquid water content, which is also sampled along the POLDER swath (Figure 1). Despite the expected fact that the LWP calculated from τ and r_e gives larger values than the directly computed LWP, it is remarkable that there is a very good correlation between the two LWPs (with a correlation coefficient of 0.98). We can therefore use this retrieved LWP to compare with POLDER-estimated LWP and perform statistics at constant LWP (as done in the following section).

4. Cloud Droplet Radius to Aerosol Index Relationship

[17] Figure 2 shows the cloud droplet effective radius (CDR) to aerosol index (AI) relationships separately for land and ocean conditions. For the POLDER data, a negative correlation is found over oceans. Over land, a negative correlation is found as well, but it is much less pronounced. For relatively large aerosol indices, almost no correlation between aerosol burden and CDR is observed. Slopes of the relationships are calculated from linear regressions between the logarithms of r_e and $\alpha\tau$ (with aerosol indices from 0.0125 to 0.40). We find $s = -0.042$

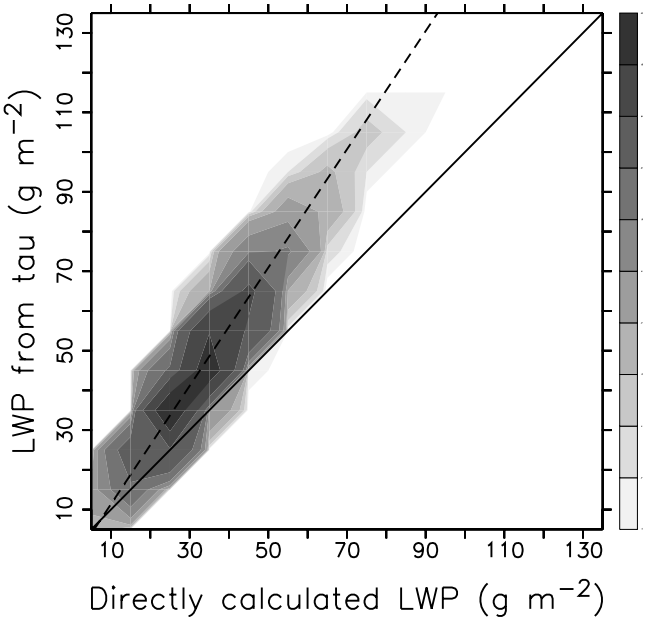

Figure 1. Joint density probability function (arbitrary units) of the LWP (in g m^{-2}) calculated from cloud optical thickness and cloud droplet effective radius (y axis) and the LWP directly calculated in the model (same units). The correlation coefficient is 0.98, and the slope of the regression line is 1.45.

for maritime and $s = -0.012$ for continental conditions. Over the ocean, *Bréon et al.* [2002] give a slope of $s = -0.085$, which is twice steeper than the one found in our study. This is due to a large extent to the averaging over a GCM grid box, where different cloud and aerosol situations are mixed. Note that over land the aerosol index retrieval is not as reliable as over the ocean (over oceans, reflectance and polarization is used for the derivation whereas over land, only polarization can be used), preventing a definite interpretation of the differences in slope. In our model, a clear relationship exists and the slope is $s = -0.092$ and -0.097 for land and ocean regions, respectively. In contrast to the CDR to AI relationship in the observations, the model simulates an impact of aerosols on the cloud droplet size also at large aerosol indices.

[18] A problem might arise because although we limit the analysis to homogeneous liquid water clouds, all LWP situations are taken into account. A correlation between CDR and AI might therefore be fortuitous if large aerosol burdens and low liquid water paths coincided. This could be the case since sources of fine-mode aerosols are located over land where the air is on average dryer. Strictly speaking, the first AIE is defined as the CDR to AI correlation at constant cloud liquid water content (or equivalently constant LWP conditions). In order to examine the first AIE in this way, we classify all situations in model results and observations into 20 LWP bins, with LWPs ranging between 0 and 200 g m^{-2}, and the number of observations equally distributed between the bins. Figure 3 shows a histogram of the LWP in model and observations. The size of the LWP bins used is also indicated on the figure. It can be seen that the distribution of LWP is shifted to larger values in the model, which is a problem in other models as well [e.g., *Suzuki et al.*, 2004]. The CDR to AI relationship is established for each LWP bin and is shown in Figure 4 for the POLDER data and the model results. In the observational data, the slopes become slightly flatter with increasing LWP. Over land, s even becomes slightly positive for very large LWP values. A reason for the decrease in the negative slope of the CDR to AI relationship may be that for thick clouds the size of the droplets at cloud top may be controlled by the available water rather than by the aerosol concentration. For the model there is no clear variation of the slope as a function of LWP. For small LWP (up to 60 g m^{-2}) over the ocean the slope becomes less negative. For LWPs between 60 and 100 g m^{-2} the slopes become steeper with increasing LWP and approach a rather constant value of -0.13 for LWP larger than 100 g m^{-2}. Over land a flattening of the slope is found for LWPs larger than 50 g m^{-2}, and s approaches a value similar to that found over the ocean at very large LWPs.

[19] In Figure 5, we compare the slopes simulated by the model with the observed slopes for different situations. We calculate the slopes for the 20 LWP bins (for the whole period and for the whole globe, Figure 5a) and the slopes for 24 regions of 15° × 7.5° on the globe (for the whole period and for all LWP, Figure 5b). In general, the

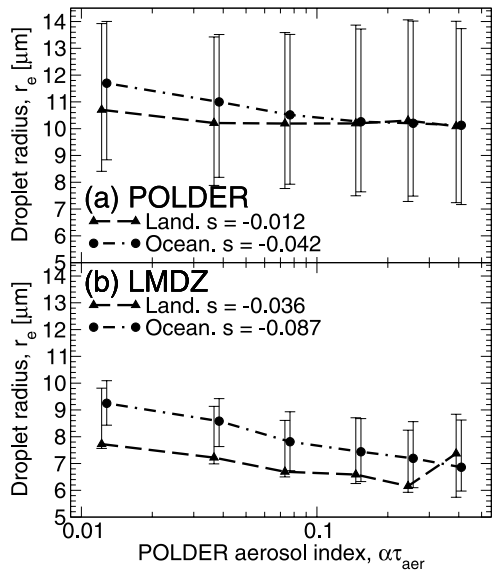

Figure 2. Relationships between cloud droplet effective radius and aerosol index for the months of December 1996 to June 1997 (for all LWP conditions) for (a) POLDER observations and (b) LMDZ model outputs. Land (triangles and long-dashed lines) and ocean (circles and dash-dotted lines) grid boxes are separated. The analysis is restricted to the region 40°S to 60°N, as POLDER observations of cloud optical thickness are not reliable at higher latitudes because of an influence of snow-covered surfaces. Error bars show the mean absolute deviation for CDR larger and smaller than the mean value within each bin of aerosol index, each bin containing $\sim 10^3$–10^5 points. For the sake of readability, the two graphs for land and ocean are slightly shifted along the x axis.

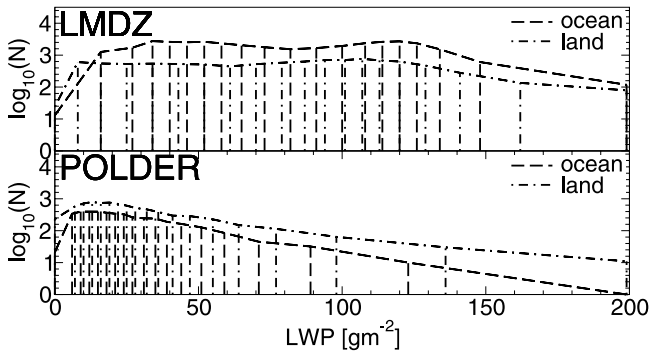

Figure 3. Histogram of the LWP in model and observations. Vertical lines indicate the bounds of the LWP bins.

model simulates too negative slopes for the CDR to AI relationship. The model always shows a negative correlation between CDR and AI, while in the POLDER observations, in particular over land, positive correlations may occur. There is a considerable scatter in Figure 5b, showing that the regional skills of the model are still limited.

[20] The slopes are in a range of [−0.15, −0.02] for the model and [−0.08, +0.01] for the observations. Except for the positive values observed in POLDER data for continental conditions, our slopes found for both model and observations are comparable to those given by *Feingold et al.* [2003], who used ground-based remote sensing measurements at different sites. In their study, values of [−0.16, −0.02] were observed. *Nakajima et al.* [2001] found a slope of −0.17 over oceans on a global scale, which is much larger than the mean values of −0.10 and −0.04 that we derived for the LMDZ model and POLDER data, respectively.

[21] *Rosenfeld and Feingold* [2003] tried to explain the differences in the slopes derived from POLDER [*Bréon et al.*, 2002] and AVHRR [*Nakajima et al.*, 2001] by arguing that POLDER preferably measures the CDR in relatively thin and homogeneous clouds with weak turbulence, whereas AVHRR results are more focused on convective and thick clouds. Thus, for the comparison with a GCM, the use of POLDER rather than AVHRR data is reasonable, as the model also assumes homogeneous clouds with a constant CDR in each layer. From our finding that the slope of the CDR to AI relationship derived at the coarse GCM resolution is half of that given by Bréon et al. at the data resolution of 150 × 150 km^2, we suggest that another reason for the difference between POLDER and AVHRR data is the fact that Nakajima et al. use an even finer resolution of 0.5° × 0.5°. Another reason for the difference is that Bréon et al. use instantaneous values, whereas Nakajima et al. look at monthly mean data, which tend to give larger slopes (see section 6 and *Sekiguchi et al.* [2003]). We may also comment on the remark by *Rosenfeld and Feingold* [2003] concerning the LWP that we did not find a large influence of stratifying or not stratifying the data by LWP.

[22] It is interesting to note that for the model the slope values s are of the order of one third (i.e., $\partial \log r_e / \partial \log N_d$) of the slope value implied by the constant $a_1 = 0.41$ in equation (2) between log N_d and log m_a. This is because of the general linear relationship between m_a and $\alpha\tau$ in the model. A similar relationship has been proposed by *Nakajima et al.* [2001] between the aerosol column number concentration, N_a, and $\alpha\tau$.

5. Cloud Liquid Water Path to Aerosol Index Relationship

[23] Examining the LWP to aerosol index relationship gives us some insight in the behavior of the second indirect effect. If the second aerosol indirect effect is real, larger LWP would be expected in regions with large aerosol concentrations. Although a correlation is not proof of the second aerosol indirect effect, one would rather expect a negative correlation in the absence of second AIE because large AI in dry continental air masses and low AI in humid maritime air masses may be associated with thin and thick clouds, respectively. In Figures 6 and 7, we plot the dependency of the LWP on aerosol index. For both the observations and the model, LWP is calculated by inverting equation (1), considering large-scale liquid water clouds only, for which a cloud droplet effective radius is defined. LWP values larger than 150 g m^{-2} are excluded from the analysis, because POLDER measurements of cloud optical thicknesses resulting in such large LWPs may be erroneous because of contamination by snow-covered surfaces (the LWP to AI relationship including all LWPs shows a very strong increase in LWP with increasing AI). While Figure 6 shows the LWP to AI relationship for 40°S to 60°N region, we restrict the analysis in Figure 7 to Northern Hemisphere (NH) midlatitudes (30°–60°N) where the AIEs are expected to be very strong. Both the observations and the model show an increase in LWP as a function of aerosol index which is statistically significant at very high confidence levels (>95%) according to the Kendall rank correlation test [*Conover*, 1980].

[24] For the 40°S to 60°N region in POLDER observations, the relationship is much less steep for continental compared to maritime conditions for AI values larger than

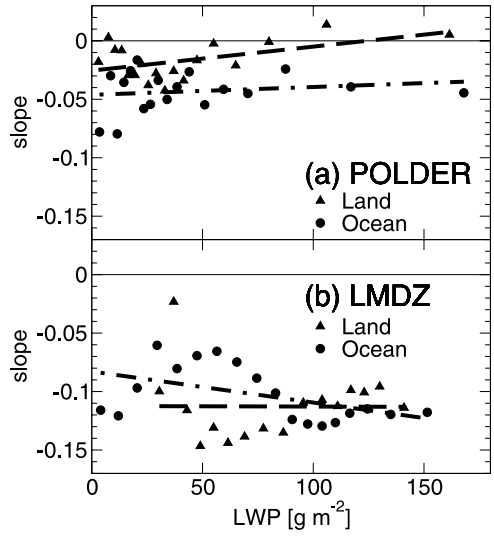

Figure 4. Slope of the CDR to AI relationship, s, as a function of LWP, for (a) the POLDER observations and (b) the LMDZ model. Ocean and land regions are shown as circles and as triangles, respectively.

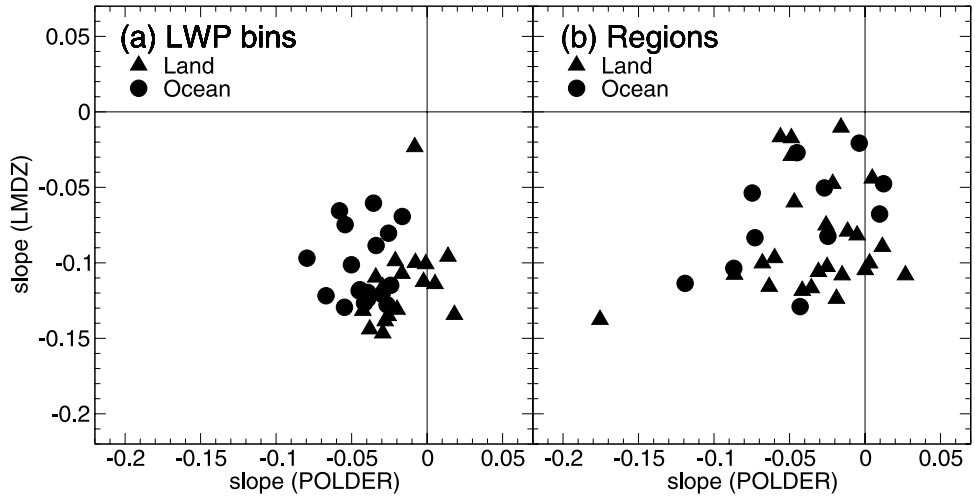

Figure 5. Scatterplot of the slope s in the model and observations for (a) the 20 LWP bins and (b) the twenty-four $15^\circ \times 7.5^\circ$ regions in the globe. Circles and triangles are for ocean and land regions, respectively.

0.1. Although an investigation of this process is beyond the scope of this study, one could argue that a semidirect aerosol effect may play a role, which reduces cloudiness in regions with large concentrations of absorbing aerosols [*Ackerman et al.*, 2000]. A further analysis shows that the LWP to AI slope is the smallest in the region 0°–30°N. Other influences may play a role as well. For example, *Feingold* [2003] shows that the relationship between CDR and aerosol extinction becomes flatter with decreasing updraft velocity for large aerosol extinctions. It is also interesting to note that in the POLDER data, and in some cases in the model simulations, the LWP to AI relationship shows slightly negative correlation at very small AI (for the first two $\alpha\tau$ bins). This could be due to the coincidence of low aerosol concentrations and large LWP values, for example in remote maritime areas.

[25] The positive correlation is even more pronounced when looking at NH midlatitudes only (Figure 7). The slopes of the LWP to AI relationship in model and observations are of the same magnitude. However, the positive slope occurs for $\alpha\tau > 0.1$ in the observations whereas it is observed throughout the range of AI in the model.

6. Indirect Effects of Anthropogenic Aerosols

[26] We performed two more experiments to further test the specific influence of anthropogenic aerosols. The control simulation is referred to as PD/PD (''present-day/present-day''), indicating that the present-day aerosol concentrations are taken in both the radiation and precipitation schemes. Anthropogenic aerosols act on the first and second AIE through these two parameterizations, respectively. In the PD/PI (''present-day/preindustrial'') experiment anthropogenic aerosols influence only the radiation parameterization while a precalculated monthly mean preindustrial aerosol distribution is used for the precipitation scheme. In the PI/PI (''preindustrial/preindustrial'') experiment anthropogenic sources were switched off in the aerosol model and preindustrial aerosol contributions are used for the first and second AIE.

[27] Figure 8 compares the PD/PD and PD/PI experiments. The impact of the second AIE on the CDR to $\alpha\tau$ relationship is relatively small: The slope is slightly steepened at large AI (Figure 8a). As shown in the previous section, LWP increase with increasing $\alpha\tau$ is largest for $\alpha\tau$ values larger than 0.1. Accordingly, we observe an impact of the second AIE on the CDR to $\alpha\tau$ relationship only at very large $\alpha\tau$ values.

[28] To compare this finding directly to the results of *Lohmann and Lesins* [2002], we redid this analysis with a different model setup (Figure 9). Here, monthly mean model data are used rather than instantaneous values, and

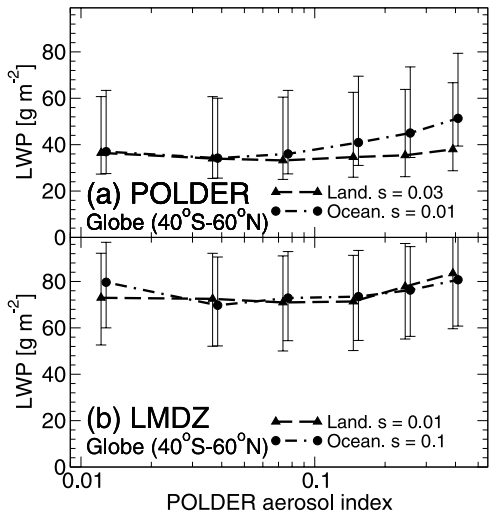

Figure 6. Cloud liquid water path to aerosol index relationships over ocean (dash-dotted lines and circles) and land (long-dashed lines and triangles) for (a) POLDER observations and (b) LMDZ model calculations. The region is restricted to 40°S to 60°N, and very large LWP values (>150 g m^{-2}) are excluded. The error bars indicate the mean absolute deviations within each bin.

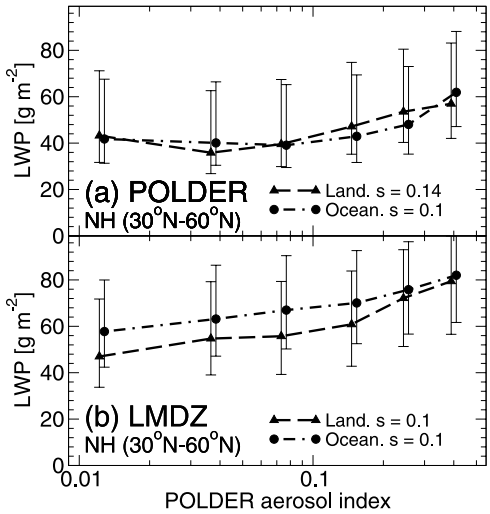

Figure 7. As in Figure 6, but for midlatitudes of the Northern Hemisphere.

a vertically varying but otherwise constant "preindustrial" cloud droplet number concentration is prescribed in the model. It should first be noted that the slope of the CDR to AI relationship derived from the POLDER data is about twice as large as it was with instantaneous values (this is also true for model values). Similar to Lohmann and Lesins' finding with the ECHAM model, we observe a correlation between CDR and AI which is purely geographically based (curve "none" without applying aerosol indirect effects). We also confirm their finding that the slope of the CDR to AI relationship is much steeper in the case where no second aerosol indirect effect is applied compared to the case where we use both aerosol indirect effects in the model.

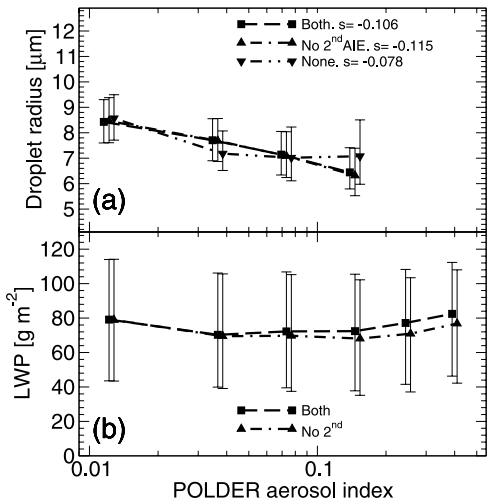

Figure 8. (a) Relationships between CDR and AI for the PD/PD control (squares and long-dashed line), PD/PI (upward pointing triangles and dash-dotted line), and PI/PI (downward pointing triangles and dot-dot-dashed line) experiments. (b) Relationships between LWP and AI for the PD/PD (squares and long-dashed line) and PD/PI (triangles and dash-dotted line) experiments. The error bars indicate the mean absolute deviation within each bin. No constraint on LWP is applied.

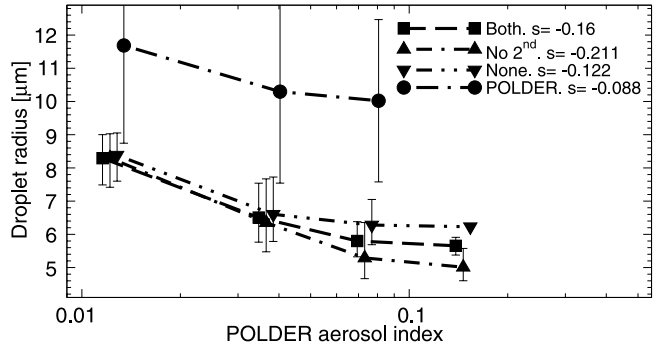

Figure 9. As in Figure 8a, but with monthly mean values and a constant "pre-industrial" CDNC applied as done by *Lohmann and Lesins* [2002]. The relationship derived from monthly mean POLDER observations is shown as circles.

[29] Figure 8a also shows the CDR to AI relationship in the PI/PI simulation using the preindustrial AI value on the x axis. The PI/PI curve shows that one should also expect a correlation between CDR and AI in preindustrial conditions. The slope of the relationship is comparable to those obtained when using present-day aerosol conditions. The existence of a positive slope is therefore not by itself proof of an anthropogenic impact; it has to be combined with an increase in aerosol index as well to produce an anthropogenic AIE.

[30] Finally, Figure 8b shows the LWP to AI relationships. Here, an impact of the second aerosol indirect effect caused by anthropogenic aerosols can clearly be identified by looking at the difference between the PD/PD and PD/PI curves. While there is no additional impact of anthropogenic aerosols on the second AIE for small aerosol indices, there is a strong anthropogenic contribution at AI larger than 0.1.

7. Summary and Conclusions

[31] Using satellite-derived data from the POLDER instrument and model simulations with the LMDZ GCM, we investigated the first and second AIE. We established relationships between aerosol index and cloud top CDR for homogeneous liquid water clouds. In both observations and model, a decrease in CDR with increasing AI is found. In the observations, this decrease is less pronounced at large AI values. When establishing the CDR to AI relationship at fixed cloud liquid water path (LWP) a similar relationship is found. However, with fixed LWP, the decrease in CDR is also found in the observations at large AI. This difference to the relationship in the case of all LWP conditions is an indication of the impact of the second AIE on the CDR to AI relationship. The slopes of the relationship are -0.01 and -0.04 for the observations over land and ocean, respectively, and -0.09 and -0.10 for the model over land and ocean, respectively.

[32] The slope of the CDR to AI relationship is found to become flatter with increasing LWP in the observations, while it approaches an almost constant value of about -0.13 for the model. In general, the model simulates too steep

slopes compared to the POLDER data. The slopes found for different regions, LWPs, and periods are, however, comparable to those given by other authors.

[33] To investigate the second AIE, we established a LWP to AI relationship. An increase in LWP with increasing AI is found for both model and observations. This increase is significant in particular for large AI ($\alpha\tau > 0.1$). A decrease in LWP with increasing AI is found at very small AI, which could be attributed to a geographical coincidence of low aerosol burden and thick clouds in remote regions. When limiting the region to Northern Hemisphere midlatitudes, the LWP to AI relationship becomes much more pronounced. These results may be interpreted as evidence for the existence of the second aerosol indirect effect on a large scale. The slope of the LWP to AI relationship in the model matches well the observations.

[34] In order to investigate the anthropogenic contribution to the aerosol indirect effects, additional experiments were carried out with the model, in which a preindustrial aerosol distribution was used for the calculation of the first and second indirect effect, respectively. We find a small impact of the anthropogenic contribution to the second AIE on the CDR to AI relationship, which is restricted to large AI values. Anthropogenic aerosols causes the CDR to decrease by 0.5 μm on average in the CDR to AI relationship. The slope, however, is hardly changed. Similarly, a small impact of anthropogenic aerosols on the LWP to AI relationship is found at large AI values. Comparing the impact of both aerosol indirect effects in our model in the same way as *Lohmann and Lesins* [2002] examined it in the ECHAM GCM, we confirm their finding that the slope of the CDR to AI relationship is much steeper when excluding the second aerosol indirect effect, and that there exists a purely geographically based correlation between CDR and AI. We find that by looking at monthly mean values one tends to overestimate the slope of the CDR to AI relationship.

[35] The comparison between model and observations provides insight in some skills and deficiencies of the model. Two shortcomings have already been widely noticed and are common to many GCMs: The CDR simulated are in general too small compared to observations by up to 3–4 μm and the LWP is too large by 10–20 g m^{-2}. The model simulates too steep slopes for the CDR to AI relationship, in particular at large AI values. In regions with large aerosol burden (the Northern Hemisphere midlatitudes), a slightly too steep dependence between LWP and AI is simulated at low AI values. We will now improve the empirical and physically based parameterizations of the model in order to obtain more realistic slopes between the various aerosol and cloud properties, which will allow us to provide ore reliable estimates of the first and second AIEs.

[36] **Acknowledgments.** Computer time was provided by the Institut de Développement et des Ressources en Informatique Scientifique (IDRIS) of the CNRS. The POLDER instrument is operated by the Centre National d'Études Spatiales (CNES).

References

Ackerman, A. S., O. B. Toon, D. E. Stephens, A. J. Heymsfield, V. Ramanathan, and E. J. Welton (2000), Reduction of tropical cloudiness by soot, *Science*, *288*, 1042–1047.

Albrecht, B. A. (1989), Aerosols, cloud microphysics, and fractional cloudiness, *Science*, *245*, 1227–1230.

Boucher, O., and J. Haywood (2001), On summing the components of radiative forcing of climate change, *Clim. Dyn.*, *18*, 297–302.

Boucher, O., and U. Lohmann (1995), The sulfate-CCN-cloud albedo effect: A sensitivity study with two general circulation models, *Tellus*, *Ser. B*, *47*, 281–300.

Boucher, O., H. Le Treut, and M. B. Baker (1995), Precipitation and radiation modeling in a general circulation model: Introduction of cloud microphysical processes, *J. Geophys. Res.*, *100*, 16,395–16,414.

Boucher, O., M. Pham, and C. Venkataraman (2002), Simulation of the atmospheric sulfur cycle in the Laboratoire de Météorologie Dynamique general circulation model: Model description, model evaluation, and global and European budgets, *Note Sci. de l'IPSL, 21*, edited by J.-P. Boulanger and Z.-X. Li, 26 pp., Inst. Pierre-Simon Laplace, Paris.

Bréon, F.-M., and S. Colzy (2000), Global distribution of cloud droplet effective radius from POLDER polarization measurements, *Geophys. Res. Lett.*, *27*, 4065–4068.

Bréon, F.-M., and P. Goloub (1998), Cloud droplet effective radius from spaceborne polarization measurements, *Geophys. Res. Lett.*, *25*, 1879–1882.

Bréon, F.-M., D. Tanré, and S. Generoso (2002), Aerosol effect on cloud droplet size monitored from satellite, *Science*, *295*, 834–838.

Buriez, J.-C., C. Vanbauce, F. Parol, P. Goloub, M. Herman, B. Bonnel, Y. Fouquart, P. Couvert, and G. Sèze (1997), Cloud detection and derivation of cloud properties from POLDER, *Int. J. Remote Sens.*, *18*, 2785–2813.

Conover, W. J. (1980), *Practical Nonparametric Statistics*, 2nd ed., 493 pp., John Wiley, New York.

Deuzé, J.-L., M. Herman, P. Goloub, D. Tanré, and A. Marchand (1999), Characterization of aerosols over ocean from POLDER/ADEOS-1, *Geophys. Res. Lett.*, *26*, 1421–1424.

Feingold, G. (2003), Modeling of the first indirect effect: Analysis of measurement requirements, *Geophys. Res. Lett.*, *30*(19), 1997, doi:10.1029/2003GL017967.

Feingold, G., W. L. Eberhard, D. E. Veron, and M. Previdi (2003), First measurements of the Twomey indirect effect using ground-based remote sensors, *Geophys. Res. Lett.*, *30*(6), 1287, doi:10.1029/2002GL016633.

Fouquart, Y., and B. Bonnel (1980), Computations of solar heating of the Earth's atmosphere: A new parameterization, *Contrib. Atmos. Phys.*, *53*, 35–62.

Han, Q., W. B. Rossow, J. Chou, and R. M. Welch (1998), Global survey of the relationship of cloud albedo and liquid water path with droplet size using ISCCP, *J. Clim.*, *11*, 1516–1528.

Han, Q., W. B. Rossow, J. Zeng, and R. Welch (2002), Three different behaviours of liquid water path of water clouds in aerosol-cloud interactions, *J. Atmos. Sci.*, *59*, 726–736.

Haywood, J. M., and S. R. Osborne (2004), The effect of overlying absorbing aerosol layers on remote sensing retrievals of cloud effective radius and cloud optical depth, *Q. J. R. Meteorol. Soc.*, in press.

Le Treut, H., and Z.-X. Li (1991), Sensitivity of an atmospheric general circulation model to prescribed SST changes: Feedback effects associated with the simulation of cloud optical properties, *Clim. Dyn.*, *5*, 175–187.

Li, Z.-X. (1999), Ensemble atmospheric GCM simulation of climate interannual variability from 1979 to 1994, *J. Clim.*, *12*, 986–1001.

Lohmann, U., and G. Lesins (2002), Stronger constraints on the anthropogenic indirect aerosol effect, *Science*, *298*, 1012–1015.

Lohmann, U., and G. Lesins (2003), Comparing continental and oceanic cloud susceptibilities to aerosols, *Geophys. Res. Lett.*, *30*(15), 1791, doi:10.1029/2003GL017828.

Morcrette, J.-J. (1991), Evaluation of model-generated cloudiness: Satellite-observed and model-generated diurnal variability of brightness temperature, *Mon. Weather Rev.*, *119*, 1205–1224.

Nakajima, T., A. Higurashi, K. Kawamoto, and J. E. Penner (2001), A possible correlation between satellite-derived cloud and aerosol microphysical parameters, *Geophys. Res. Lett.*, *28*, 1171–1174.

Rayner, N. A., D. E. Parker, E. B. Horton, C. K. Folland, L. V. Alexander, D. P. Rowell, E. C. Kent, and A. Kaplan (2003), Global analyses of SST, sea ice and night marine air temperature since the late nineteenth century, *J. Geophys. Res.*, *108*(D14), 4407, doi:10.1029/2002JD002670.

Reynolds, R. W., and T. M. Smith (1995), A high-resolution global sea surface temperature climatology, *J. Clim.*, *8*, 1571–1583.

Rosenfeld, D., and G. Feingold (2003), Explanation of discrepancies among satellite observations of the aerosol indirect effects, *Geophys. Res. Lett.*, *30*(14), 1776, doi:10.1029/2003GL017684.

Schwartz, S. E., Harshvardhan, and C. M. Benkovitz (2002), Influence of anthropogenic aerosol on cloud optical depth and albedo shown by satellite measurements and chemical transport modeling, *Proc. Natl. Acad. Sci. U. S. A.*, *99*, 1784–1789.

Sekiguchi, M., T. Nakajima, K. Suzuki, K. Kawamoto, A. Higurashi, D. Rosenfeld, I. Sano, and S. Mukai (2003), A study of the direct and indirect effects of aerosols using global satellite data sets of aerosol

and cloud parameters, *J. Geophys. Res.*, *108*(D22), 4699, doi:10.1029/2002JD003359.
Stephens, S. E. (1978), Radiation profiles in extended water clouds. II: Parameterization schemes, *J. Atmos. Sci.*, *35*, 2123–2132.
Suzuki, K., T. Nakajima, A. Numaguti, T. Takemura, K. Kawamoto, and A. Higurashi (2004), A study of the aerosol effect on a cloud field with simultaneous use of GCM modelling and satellite observation, *J. Atmos. Sci.*, *61*, 179–194.
Tiedtke, M. (1989), A comprehensive mass flux scheme for cumulus parameterization in large-scale models, *Mon. Weather Rev.*, *117*, 1779–1800.
Twomey, S. (1974), Pollution and the planetary albedo, *Atmos. Environ.*, *8*, 1251–1256.
Webb, M., C. Senior, S. Bony, and J.-J. Morcrette (2001), Combining ERBE and ISCCP data to assess clouds in the Hadley Centre, ECMWF and LMD atmospheric climate models, *Clim. Dyn.*, *17*, 905–922.
Wetzel, M. A., and L. L. Stowe (1999), Satellite-observed patterns in stratus microphysics, aerosol optical thickness, and shortwave radiative forcing, *J. Geophys. Res.*, *104*, 31,287–31,299.

O. Boucher, Laboratoire d'Optique Atmosphérique, UFR de Physique, Université des Sciences et de Technologie de Lille/CNRS, F-59655 Villeneuve d'Ascq Cedex, France. (boucher@loa.univ-lille1.fr)
F.-M. Bréon, Laboratoire des Sciences du Climat et de l'Environnement (IPSL/CNRS), Commissariat à l'Energie Atomique (CEA), F-91191 Gif sur Yvette Cedex, France. (fmbreon@cea.fr)
J. Quaas, Laboratoire de Météorologie Dynamique (IPSL/CNRS), Université Pierre et Marie Curie, F-75252 Paris Cedex, France. (quaas@lmd.jussieu.fr)